# Photosensitivity Characterization of Nanostructured Tin Oxide Films and Alternative Photodetector Application

Márcio Fontana, *Associate Member, IEEE*, Nilo Matias, Fabiano Fragoso Costa, *Member, IEEE*, Aiese C. Barros, and Amauri Oliveira, *Member, IEEE*

***Abstract*—In this paper, we present an analysis of the photosensitivity property of electrical resistance of nanostructured porous tin oxide films ($SnO_2$) deposited on Si substrates using a spray method. Based on this property, we propose a new application for this material as an element in a photodetector device. As we verified that the film photosensitivity is influenced by room temperature, to develop a photodetector device, we propose a microcontroller-based algorithm for compensating temperature changes in a certain range. The morphological and chemical structure of the sample films revealed by atomic force microscopy (AFM) and Raman spectroscopy are also discussed. The dynamics of the photodetector have been tested by varying the frequency of light excitation and the temperature of the film. The results show that the device works properly for intermediate ranges of frequency and temperature, but its response degrades as the frequency or temperature rises.**

***Index Terms*—$SnO_2$, photodetector, photosensitivity, tin oxide film.**

## I. Introduction

Tin dioxide ($SnO_2$) films has been applied in the last 20 years in devices such as gas sensors [1], [2] and photovoltaic cells [3], [4]. Flat-panel display devices [5], [6] and transparent electrodes [7] are among the newest and most useful applications under investigation. Regarding production, $SnO_2$ films may be grown with unique properties, such as low electrical resistivity, high optical transparency, high or low porosity, and high chemical stability. Recent studies have shown new informations on nanostructured $SnO_2$, such as the following: photoresponse of $SnO_2$ [8], photocurrent gain in $SnO_2$ nanowires [9], and nanostructrured photodetectors [10], [11]. However, the photosensitivity properties of $SnO_2$ films have not yet been investigated in detail. In [12], it was shown that the electrical resistance of $SnO_2$ films is highly sensitive in low, narrow ranges of illuminance. This feature opens the opportunity to exploit a new application for the film as part of a photodetector device.

To build a photodetector, it is necessary to turn the resistance variation into a useful signal: a voltage. This can be carried out by two approaches. The first one is to apply a voltage to a network comprised of a reference resistor and the film connected in series. This method has the inconvenience of measuring the whole voltage across the film and not only the voltage variation. Hence, in this paper, we opted to capture this variation by means of a bridge circuit [13]. As we verified that $SnO_2$ film photosensitivity was affected by temperature, we also needed to developed a compensation algorithm to cope with temperature variations.

An ideal subsystem application for a microcontroller is the acquisition, control, and conditioning of analog sensor inputs. A typical multiple-sensor system usually requires some or all of the following steps: 1) excitation, 2) multiplexing, 3) filtering, 4) A/D conversion, 5) amplification, and 6) offset and thermal compensation [14]. Whereas steps 1) to 4) are generic, i.e., no individual sensor calibration need be accomplished to design the support circuitry, the gain, offset, and thermal compensation must be individually tailored to absorb the device-to-device variations to achieve maximum performance. This is particularly true if the device variations are large and/or the sensor thermal sensitivity is high. However, the individual sensors are manually "tweaked" via trim potentiometer adjustments to remove offset errors and gain variations. The temperature compensation is accomplished with a dedicated thermally sensitive network. This approach is time proven and appropriate for a single photodetector. Thus, we adopted this method.

This paper describes the photosensitivity characterization of nanostructured porous $SnO_2$ films and the development of an alternative sensor based on a microcontroller to detect a certain intensity of light in a darkroom. This photodetector can be applied to event counting, velocity measurements, barrier sensors, encoders, etc. This paper is organized as follows. The second section describes the experimental procedures related to the film deposition process and the measurement systems for the $SnO_2$ characterization and for testing the photodetector dynamics. The third section overviews the photodetection principles used in this work. The results and discussions are presented in the fourth section, and conclusions are drawn in the last section.

Manuscript received April 29, 2010; revised July 28, 2010; accepted August 07, 2010. Date of publication September 23, 2010; date of current version February 04, 2011. This work was supported in part by the Brazilian agencies Conselho Nacional de Desenvolvimento Científico e Tecnológico (CNPQ), in part by Coordenação de Aperfeiçoamento de Pessoal de Nível Superior (CAPES), and in part by Fundação de Amparo à Pesquisa do Estado da Bahia (FAPESB). The associate editor coordinating the review of this paper and approving it for publication was Dr. M. Abedin.

M. Fontana, N. Matias, A. C. Barros, and A. Oliveira are with the Department of Electrical Engineering, Federal University of Bahia, Federação CEP 40210-630, Salvador, BA, Brazil (e-mail: mfontana@ufba.br; nilo@globaltek.com.br; aiesebarros@bol.com.br; amauri@ufba.br).

F. F. Costa is with the Department of Electrical Engineering, Federal University of Rio Grande do Norte, Lagoa Nova CEP 59072-970—Natal, RN, Brazil (e-mail: ffcosta@ufrnet.br).

Color versions of one or more of the figures in this paper are available online at http://ieeexplore.ieee.org.

Digital Object Identifier 10.1109/JSEN.2010.2068542

## II. Experimental Procedures

### A. Film Deposition

Silicon wafers (n-type, $\langle 100 \rangle$ orientation, 500–550 $\mu$m thickness, 1–10 $\Omega$cm resistivity) produced by SI-TECH, Inc., and used in this work were ultrasonically degreased in acetone and ethyl alcohol, then rinsed in distilled water and dried in hot nitrogen.

The samples were deposited using the spray pyrolysis system described in [16]. The experimental setup consisted of a reservoir of liquid Sn solution that was fed by gravity into a jet gas nozzle. The spray was induced by the flow of hydrogen through a small orifice to the atmosphere. Control valves were placed to independently adjust the hydrogen and the Sn solution flow rates. The substrates were mounted horizontally over a steel hotplate placed below the jet nozzle to receive a uniform spray coating. A 0.2 M solution of pentahydrated stannic chloride ($SNCl_4 5H_2O$) in ethanol ($C_2H_5OH$) was used in the feed reservoir. Hydrogen flow was kept at 7 lmin$^{-1}$ at 1520 Torr pressure, and the solution spray rate was around 1 ml min$^{-1}$. The deposition temperature, measured by a chromel–alumel thermocouple, was controlled via the power supplied to the hotplate and was set to 350 °C. After establishing the stability of the deposition parameters described, the substrates were introduced into the reactor for 60 s.

### B. Measurement Systems

Surface morphology of the grown layers was examined by AFM using a ThermoMicroscopes AutoProbe CP. Micro-Raman spectroscopy was carried out at ambient temperature using a RENISHAW – inVia Raman Microscope, employing the output of an Ar+ laser (5-mW power) for excitation at $\lambda = 514.5$ nm.

Each film sample, with an area of 1 cm$^2$ and a grain size around 50 nm, was mounted onto a thermoelectric module inside an isolated thermal chamber (Fig. 1). The film temperature was measured using a precision centigrade temperature sensor (LM35). A red light emitting diode (LED) source provided the incident light on the film surface. A Yokogawa DL1700E Oscilloscope was used to probe the relevant signals involved in the photodetection process, a Minipa MFG4200 Function Generator Signal was used for exciting the red LED circuit and an Agilent E3646A Dual Output Power Supply was used to bias the Thermal Electrical Mode (TEM) and control the room temperature. The measurement system is shown in Fig. 1.

A digital controller was implemented in an IEEE-488 environment using a computer to set the temperature. The computer was also used to store the data of the measurement system

## III. Photodetection Process

To build a photodetector, we conceived a circuit that directly relates the resistance variation provoked by light intensity to an electrical signal variation. At the same time, we developed an algorithm to cope with temperature variations. This was accomplished by means of a microcontroller. Fig. 2 shows the complete schematic block diagram for an alternative photodetector based on a microcontroller using $SnO_2$ films. The blocks are individually described in subsections 1) to 4).

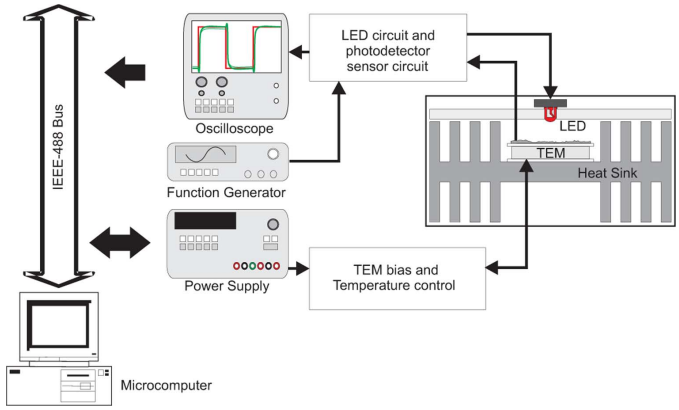


Fig. 1. Typical measurement system used to characterize the photodetector sensor.

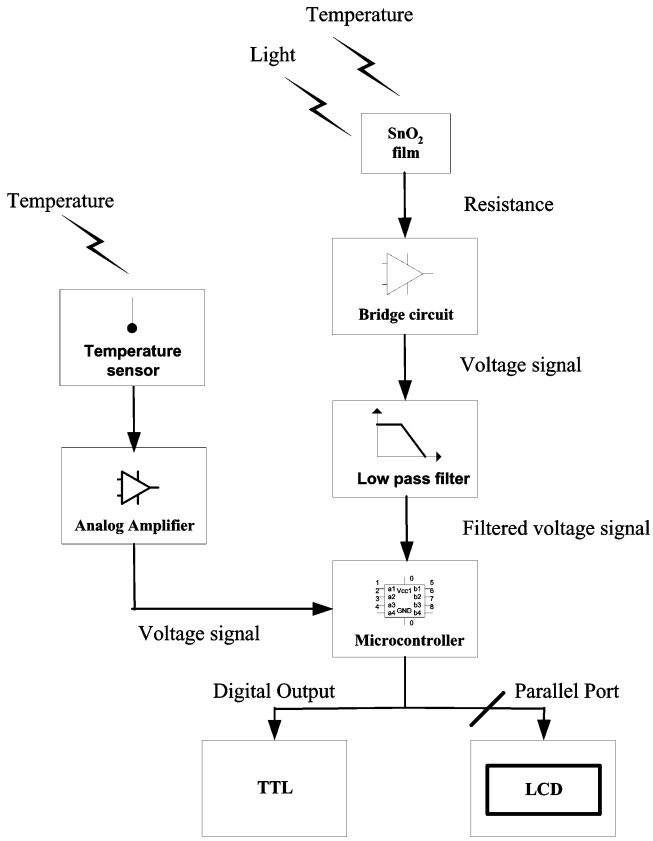


Fig. 2. Microcontroller-based photodetector sensor.

*1) $SnO_2$ Film Block:* The top block ($SnO_2$ film) in Fig. 2 represents the electrical resistance variation of the $SnO_2$ film with light intensity and temperature. The superficial resistance film is an element of a bridge circuit, represented by the bridge circuit block.

*2) Bridge Circuit and Low-Pass Filter Blocks:* We used the bridge circuit shown in Fig. 3 to convert the electrical resistance variation into a voltage signal. $R_f(T)$ represents the resistance of a $SnO_2$ film, which depends on the temperature and the incident light on the film surface. Supposing an ideal operational amplifier, the bridge output voltage $V_{ob}(T)$ is given by

$$V_{ob}(T) = \frac{R_2 R_3}{R_2(R_1 + R_3)} - \frac{R_1 V_{cc}}{R_2(R_1 + R_2)} R_f(T) \quad (1)$$

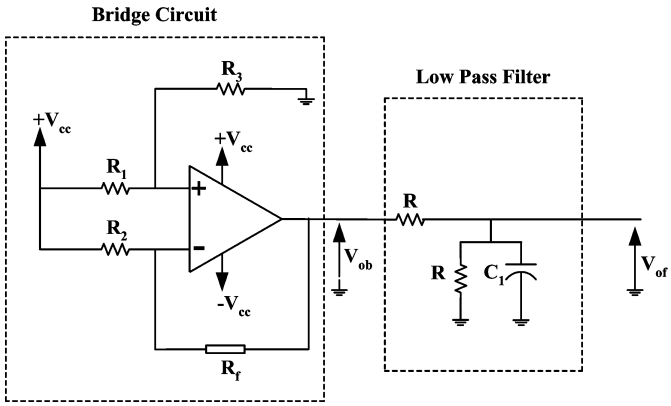


Fig. 3. Bridge circuit followed by a low-pass filter stage.

TABLE I
THRESHOLD SETUP FOR THE MICRONTROLLER

| Temperature ($^oC$) | $V_{omin}(V)$ | $V_{omax}(V)$ | Threshold (V) |
|---|---|---|---|
| 25 | 0.3 | 4.6 | 2.5 |
| 30 | 1.8 | 4.7 | 3.3 |
| 35 | 2.9 | 4.7 | 3.8 |
| 40 | 3.6 | 4.8 | 4.0 |
| 45 | 4.0 | 4.8 | 4.4 |

which also can be written as

$$V_{ob}(T) = K_1 + K_2 R_f(T) \tag{2}$$

where $K_1 = 11.4\,\text{V}$, and $K_2 = 2.4.10^{-6}\,\text{V}\cdot\Omega^{-1}$ are parameters obtained from the bridge resistances.

To reduce noise and to avoid aliasing, the signal $V_{ob}$ must be filtered. A simple $RC$ network was used as a first order low-pass filter with a transfer function given by $H(s) = V_{of}(s)/V_{ob}(s) = 1/(2 + RCs)$. The values of resistance and capacitance determine the time constant of the filter $(\tau = RC/2)$ and the cutoff frequency (in hertz) is given by

$$f_c = \frac{1}{2\pi\tau} = \frac{1}{\pi RC} \tag{3}$$

where the cutoff frequency is 2.59 kHz and the static gain is 0.5.

*3) Microcontroller Block:* The microcontroller is the element in which the signals provided by the low-pass filter and the temperature sensor are processed to supply a binary signal that should inform whether the light is ON or OFF in a given environment. To accomplish these functions an algorithm for compensating the variations in temperature had to be developed. Thus, we started by storing, in the ROM of the microcontroller, the minimum $(V_{omin})$ and the maximum $(V_{omax})$ voltage values obtained from the low-pass filter output for a set of five temperature values that were also stored in the microcontroller memory, as shown in Table I. Thus, for instance, taking the temperature value of 25 °C, when the illuminance of the incident light hitting the film surface is 0 lx, the low-pass filter output is 0.3 V. As the illuminance rises to 15 lx, the filter output changes to 4.6 V. We arbitrarily selected a medium value between $V_{omin}$ and $V_{omax}$ as a threshold to set the light sensor OFF (filter output below the threshold) or ON (filter output above the threshold). This is a reasonable option because for higher values of illuminance the film resistance is not altered significantly, as shown in Fig. 6. A temperature value between 25 °C and 40 °C imposes a threshold limit determined by a linear interpolation. For example, a temperature value of 27 °C is associated with a threshold limit $Th_x$ of 2.82 V, which is obtained through the expression

$$\frac{Th_x - 2.5}{3.3 - 2.5} = \frac{27 - 25}{30 - 25}. \tag{4}$$

For temperature values above 45 °C, the efficiency of the sensor is lost since $V_{omin}$ and $V_{omax}$ values get closer to each other. The microcontroller is a Microhip PIC16F877A that operates at 4 MHz clock frequency and performs 8-bit analog-to-digital conversions of two multiplexed input channels: channel 1 measures the voltage generated by the temperature sensor circuit while channel 0 measures the voltage signal from the bridge circuit. One transistor–transistor logic (TTL) digital output and a 16x2 LCD provides the measurement results. An RS-232 serial port allows user interface with a PC for the microcontroller configuration and to store the data history. The microcontroller reads the temperature first and then determines the threshold limit.

*4) Photodectetor Output:* The microcontroller communicates with a 16x2 LCD character via a 4-bit parallel output port. The film temperature and the light switching frequency are displayed on the LCD. In addition, a TTL output pulse with the same light switching frequency is available for the user. This signal can be applied in an external circuit for any distinct further processing, such as an external counter.

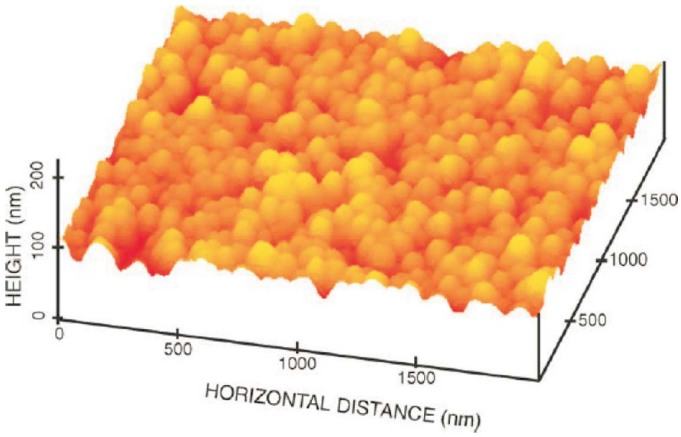


Fig. 4. AFM image of the sample deposited at 350 °C, which represents the typical morphologies of the samples as revealed by AFM.

## IV. RESULTS AND DISCUSSION

### A. AFM and Raman Spectrum Characterizations of $SnO_2$

We deposited $SnO_2$ samples at temperatures ranging from 250 °C to 450 °C. All samples were analyzed by AFM and Raman spectroscopy. We identified that $SnO_2$ samples were similar to the grain size, granular morphology, and Raman spectrum characterizations. In this way, we chose the $SnO_2$ samples deposited at 350 °C (average temperature) for the photodetector development. Fig. 4 shows the three-dimensional morphology of the $SnO_2$ sample deposited at 350 °C, which represents the typical morphologies of the samples as revealed by AFM. The

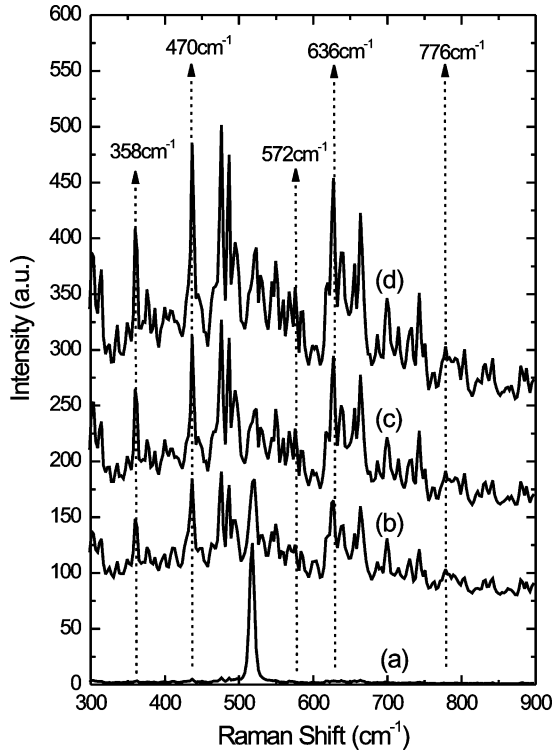


Fig. 5. Typical room-temperature Raman spectra of Si substrate [curve (a)] and $SnO_2$ samples [curves (b), (c) and (d)].

particle size at 350 °C is around 50 nm. A higher deposition temperature contributes to the increase of film roughness and to the increase in lateral particle size. We observe that the heights of the particles are nearly equal to their diameters, according to the results obtained in [15].

Fig. 5 shows the typical room-temperature Raman spectrum of the Si substrate [curve (a)] and three similar $SnO_2$ samples [curves (b), (c), and (d)]. These last three results conform to those observed in [17]. According to this work, the Raman spectrum may be divided into two groups. In the first group, the Raman peaks are the same as those from single-crystal or polycrystalline $SnO_2$. The three Raman peaks are located at 470, 636, and 776 $cm^{-1}$. These peaks are close to the frequencies of three active Raman vibrational modes ($E_g$, $A_{1g}$ and $B_{2g}$) of crystalline and microcrystalline $SnO_2$ tetragonal rutile structures, which have been experimentally observed at 474, 632, and 774 $cm^{-1}$ in [18]. The peaks from the second group, observed in [17], are located at 358 and 572 $cm^{-1}$. These two peaks are not observed in Raman spectra of single-crystal and polycrystalline $SnO_2$, and they are only observed in nanometer $SnO_2$ grains and are attributed to the effect of Raman surface modes that dominate at the nanoscale [19]. However, we also observe, in Fig. 5, Raman peaks of SnO, $SnO_2$, and $Sn(OH)_2$, $Sn(OH)_4$ among other peaks. The presence of these peaks is probably justified by the interaction between tin and silicon or tin and silicon oxide.

### B. Photosensitivity Characterization of $SnO_2$

Fig. 6 illustrates the dependence of electrical resistance on illuminance for a $SnO_2$ film. To obtain the curve, a red light-emitting diode source provided the incident light on the film surface,

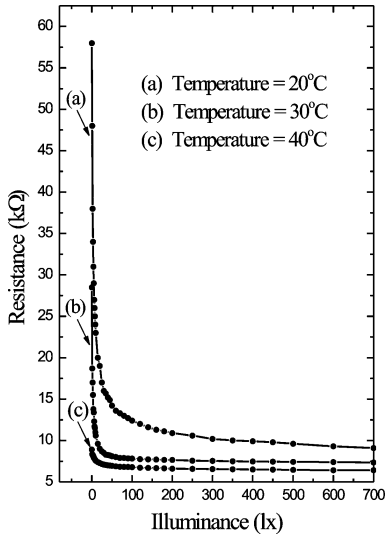


Fig. 6. Electrical resistance dependence on illuminance and temperature.

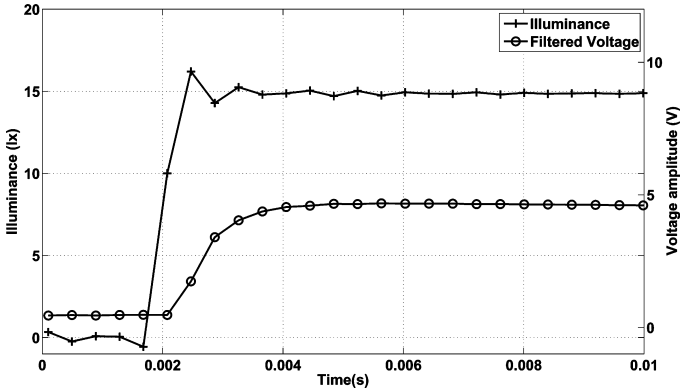


Fig. 7. Typical step response of the photodetector sensor with temperature control (at 25 °C).

which served as the excitation for the film. We verified that this dependence is parameterized by the temperature to which the film is submitted; three curves associated with the temperature values of 20 °C, 30 °C, and 40 °C are presented in Fig. 6.

We also note that for the range between 0 and 200 lx the film shows higher sensitivity. In fact, we have previously demonstrated that the sensitivity of this kind of films is related to the temperature needed for efficient thermal decomposition of the hydroxides to form n-type $SnO_2$ nanocrystals [12].

### C. Photodetector Dynamic

Fig. 7 shows the photodetector response for a step excitation of current into the LED. The illuminance of the incident light hitting the $SnO_2$ surface is proportional to the current intensity (1.5 lx corresponds to 1 mA of current). The film temperature was set to 25 °C. Observing the response's shape going to 4.5 V, we can infer that the photodetector resembles an overdamped second-order system associated with a rise-time of approximately 2 ms and a dead-time of 0.4 ms. For the present application, this response is adequate.

Fig. 8 illustrates the influence of the room temperature over the photodetector response for a pulse excitation. The pulse frequency was set at 50 Hz and the illuminance at 15 lx. We can

TABLE II
EXPERIMENTAL MICROCONTROLLER COUNTING

| LIF (Hz) | Temperature=25 $^oC$ | | Temperature=30 $^oC$ | | Temperature=35 $^oC$ | | Temperature=40 $^oC$ | | Temperature=45 $^oC$ | |
|---|---|---|---|---|---|---|---|---|---|---|
| | Max (Hz) | Min (Hz) | Max (Hz) | Min (Hz) | Max (Hz) | Min (Hz) | Max (Hz) | Min (Hz) | Max (Hz) | Min(Hz) |
| 20 | 20 | 19 | 21 | 19 | 20 | 20 | 20 | 20 | 21 | 23 |
| 40 | 40 | 39 | 41 | 40 | 40 | 40 | 40 | 40 | 44 | 41 |
| 60 | 60 | 60 | 61 | 60 | 60 | 60 | 60 | 60 | 62 | 60 |
| 80 | 81 | 79 | 81 | 80 | 80 | 79 | 80 | 80 | 81 | 80 |
| 100 | 100 | 100 | 102 | 100 | 100 | 99 | 100 | 100 | 101 | 100 |

LIF=Light Input Frequency

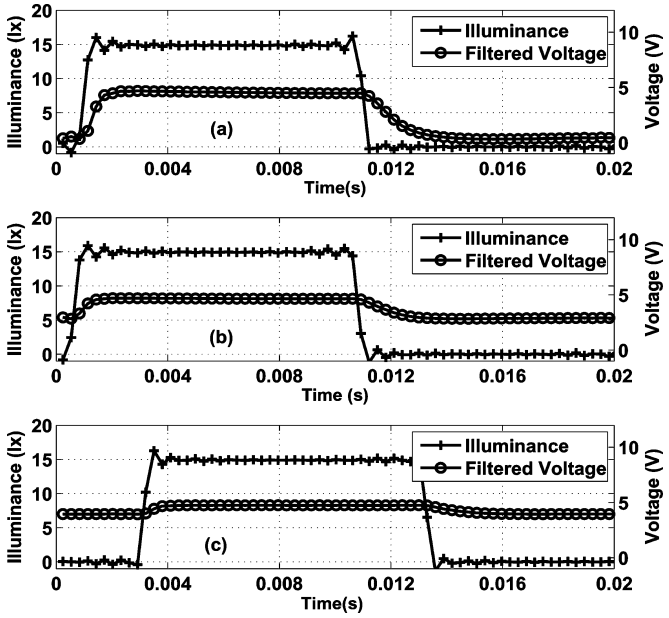


Fig. 8. Typical photodetector sensor response for a square-wave excitation: (a) temperature $= 25$ °C; (b) temperature $= 35$ °C; and (c) temperature $= 45$ °C.

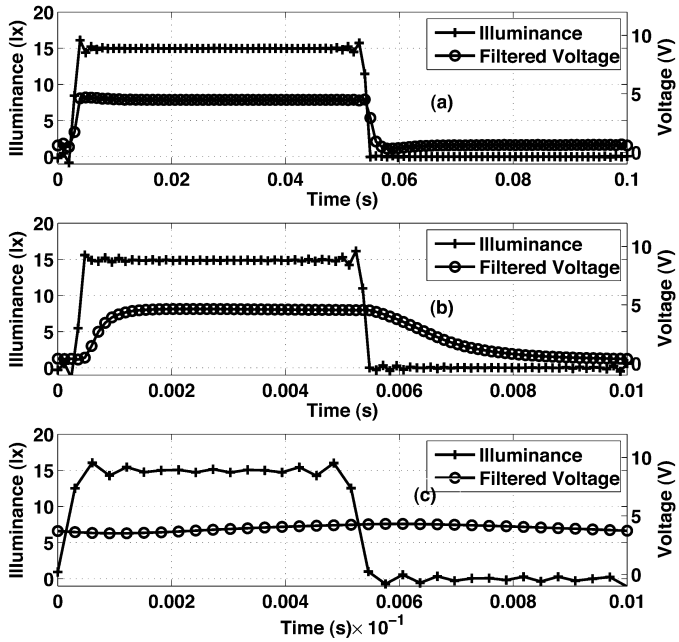


Fig. 9. Typical photodetector response for excitations at different frequencies: (a) 10 Hz; (b) 100 Hz; and (c) 1000 Hz.

note that, as the temperature rises, the lower level of the filtered voltage drifts upwards while the upper level remains approximately the same. Because the upper level is obtained when the light is ON, this suggests that the photosensitivity phenomenon of the $SnO_2$ films dominates over the temperature phenomenon. This is consistent with the results presented in Fig. 6, where the resistance variation related to temperature variation is greater under the dark condition (0 lx). For the temperatures ranging from 25 °C to 45 °C, the thermal effect poses no problem for the photodetector's operation. The difference between the upper and lower levels is still around 1.0 V, which is enough for the bit resolution of most microcontrollers. Even so, a temperature compensation algorithm was developed in this work to cope with higher temperatures.

Fig. 9 shows the photodetector behavior when the film is submitted to pulse excitations of three different frequencies. It can be noted that, at the lower frequency, 10 Hz, the pulse response (filtered voltage) presents two clearly distinguishable levels. As the frequency rises to 100 Hz and 1000 Hz, the upper and lower levels can be misinterpreted by the microcontroller because they get too close to each other. Therefore, this limitation must be taken into account for applications that require a fast response.

To show the effectiveness of the compensation algorithm for temperature variation, the microcontroller was programmed as a pulse counter. The pulse counter was tested for frequencies of light input excitation ranging from 20 to 100 Hz and for temperature values ranging from 25 °C to 45 °C. For each temperature and frequency value, we ran the pulse counter ten times, each of them for 2 s. Table II shows the maximum and minimum values of the counting obtained for the ten times. Observe that the unit of the counts is $n^o pulses/second =$ Hz. The results are satisfactory for the considered range of temperatures and frequencies.

## V. CONCLUSION

In this paper, we examined the photosensitivity of the electrical resistance of nanostructured porous tin oxide films. In addition, we verified that photosensitivity is also dependent on the temperature. The photosensitivity property allowed us to propose a new application for these films as part of photodetector systems. Hence, a microcontroller-based algorithm was developed to compensate for temperature changes. The results show that the photodetector response degrades as the temperature of the film and frequency of the input excitation rise. Nevertheless, its performance in intermediate ranges of temperature and excitation frequency justifies further research in sensors based on $SnO_2$ films.

## ACKNOWLEDGMENT

The authors would like to thank Dr. H. J. Ceragioli and Dr. A. C. Peterlevitz from FEEC/UNICAMP for their technical assistance. They would also like to thank LABSIF/FEEC/UNICAMP for use of their Raman spectrometer.

## REFERENCES

[1] L. Sangaletti, L. E. Depero, A. Dieguez, G. Marca, J. R. Morante, A. R. Rodriguez, and G. Sberveglieri, "Microstructure and morphology of tin dioxide multilayer thin film gas sensors," *Sens. Actuat. B-Chem.*, vol. 44, no. 1–3, pp. 268–274, 1997.

[2] J. G. Partridge, M. R. Field, A. Z. Sadek, K. Kalantar-Zadeh, J. Du Plessis, M. B. Taylor, A. Atanacio, K. E. Prince, and D. G. McCulloch, "Fabrication, structural characterization and testing of a nanostructured Tin Oxide gas sensor," *IEEE Sens. J.*, vol. 9, pp. 563–568, May 2009.

[3] O. H. Winn, S. L. Franz, and R. L. Anderson, "Static optoelectronic characteristics of $SnO_2/V_2O_5 : P_2O_5/Si$ heterojunctions," *J. Appl. Phys.*, vol. 50, no. 5, pp. 3758–3761, 1979.

[4] L. T. Yin, J. C. Chou, W. Y. Chung, T. P. Sun, and S. K. Hsiung, "Separate structure extended gate $H^+ - ion$ sensitive field effect transistor on a glass substrate," *Sens. Actuat. B-Chem.*, vol. 71, no. 1–2, pp. 106–111, 2000.

[5] S. J. Laverty and P. D. Maguire, "Low resistance transparent electrodes for large area flat display devices," *J. Vac. Sci. Technol.*, vol. 19, no. 1, pp. 1–6, 2001.

[6] V. Brinzari, G. Korotcenkov, and V. Golovanov, "Factors influencing the gas sensing characteristics of tin dioxide films deposited by spray pyrolysis: Understanding and possibilities of control," *Thin Solid Films*, vol. 391, no. 2, pp. 167–175, 2001.

[7] A. C. Arias, L. S. Roman, T. Kugler, R. Toniolo, M. S. Meruvia, and I. A. Hmmelgen, "The use of tin oxide thin films as a transparent electrode in PPV based light-emitting diodes," *Thin Solid Films*, vol. 371, no. 1–2, pp. 201–206, 1979.

[8] Y. J. Chen, C. L. Zhu, M. S. Cao, and T. H. Wang, "Photoresponse of $SnO_2$ nanobelts grown *in situ* on interdigital electrodes," *Nanotechnology*, vol. 18, no. 28, pp. 285502:1–285502:5, 2007.

[9] C. H. Lin, R. S. Chen, T. T. Chen, H. Y. Chen, Y. F. Chen, K. H. Chen, and L. C. Chen, "High photocurrent gain in $SnO_2$ nanowires," *Appl. Phys. Lett.*, vol. 93, no. 11, pp. 112115:1–112115:3, 2008.

[10] T. Zhai, X. Fang, M. Liao, H. Zeng, B. Yosho, and D. Golberg, "A comprehensive review of one-dimensional metal-oxide nanostructure photodetectors," *Sensors*, vol. 9, no. 8, pp. 6504–6529, 2009.

[11] T. Zhai, X. Fang, M. Liao, X. Xu, L. Li, B. Liu, Y. Koide, Y. Ma, J. Yao, Y. Bando, and D. Golberg, "Fabrication of high-quality $In_2Se_3$ nanowire arrays toward high-performance visible-vight photodetectors," *ACS Nano*, vol. 4, no. 3, pp. 1596–1602, 2009.

[12] M. Fontana, N. Matias, A. C. Costa, F. F. Costa, and A. Oliveira, "Characterization of photosensitivity of eletrical resistance of nanostructured pourous tin oxide films deposited from spray method," in *Proc. 17th Annu. Int. Conf. Composites/Nano Eng.—ICCE—17*, Honolulu, HI, 2009, vol. 1, pp. 1–2.

[13] S. Gal, G. Cathkbras, and Y. Bertrand, "Measurement of small resistance variations using technique," *Eletron. Lett.*, vol. 34, no. 16, pp. 1578–1579, 1998.

[14] P. T. Kolen, "Self-calibration/compensation technique for microcontroller-based sensor arrays," *IEEE Trans. Instrum. Meas*, vol. 43, no. 4, pp. 620–624, Aug. 1994.

[15] V. Baranauskas, M. Fontana, Z. J. Guo, H. J. Ceragioli, and A. C. Peterlevitz, "Field-emission properties of nanocrystalline tin oxide films," *Sens. Actuat. B-Chem.*, vol. 107, no. 1, pp. 474–478, 2005.

[16] F. C. Marques, "Sprayed $SnO_2$ antireflection coating on textured silicon surface for solar cell applications," *IEEE Trans. Electron Devices*, vol. 45, no. 7, pp. 1619–1621, Jul. 1998.

[17] J. Zuo, C. Xu, X. Liu, C. Wang, C. Wang, Y. Hu, and Y. Qian, "Study of the Raman spectrum of nanometer $SnO_2$," *J. Appl. Phys.*, vol. 75, no. 3, pp. 1835–1836, 1994.

[18] S. H. Sun, G. W. Meng, G. X. Zhang, T. Gao, B. Y. Geng, L. D. Zhang, and J. Zuo, "Raman scattering study of rutile $SnO_2$ nanobelts synthesized by thermal evaporation of Sn powders," *Chem. Phys. Lett.*, vol. 376, no. 1–2, pp. 103–107, 2003.

[19] A. Dieguez, A. Romano-Rodriguez, J. R. Morante, U. Weimar, M. Schweizer-Berberich, and W. Gopel, "Morphological analysis on nanocrystalline $SnO_2$ for gas sensor applications," *Sens. Actuat. B-Chem.*, vol. 31, no. 1–2, pp. 1–8, 1996.

[20] M. Ocana, C. J. Serna, and J. V. Garcia-Ramos, "A vibrational study of uniform $SnO_2$ powders of various morphologies," *Solid State Ionics*, vol. 63–65, pp. 170–177, 1993.

**Márcio Fontana** (A'07) was born in Criciúma, Santa Catarina, Brazil, in 1975. He received the B.S. degree in electrical engineering from the State University of Santa Catarina (UDESC) in 1999, the M.S. degree in electrical engineering from the Federal University of Paraíba (UFPB), João Pessoa, Brazil, in 2001, and the Ph.D. degree in electrical engineering from the State University of Campinas (UNICAMP), Campinas, Brazil, in 2004.

In September 2004, he joined as Assistant Professor the Department of Electrical Engineering, Federal University of Bahia (UFBA), Salvador, Brazil, where he has been working in the field of electrical materials focusing in nanostructured materials.

**Nilo Matias** received the M.S. degree in electrical engineering from the Federal University of Bahia (UFBA), Salvador, Brazil, in 2009.

His current interests are in new materials, sensors, and signal processing for measuring purposes.

**Fabiano Fragoso Costa** (M'07) received the B.S., M.S. and Ph.D. degrees from University of São Paulo (USP), Federal University of Paraíba (UFPB) and University of Campina Grande (UFCG) in 1997, 2001 and 2005 respectively, all in electrical engineering. He is presently an Assistant Professor at the Department of Electrical Engineering in Federal University of Rio Grande do Norte (UFRN). His research interests include digital signal processing, power quality and modeling of dynamic systems.

**Aiese C. Barros** is currently pursuing the B.S. degree in electrical engineering at the Federal University of Bahia (UFBA), Salvado, Brazil.

His research interests are in electronic instrumentation.

**Amauri Oliveira** (M'88) received the B.S. degree from the Federal University of Bahia (UFBA), Salvador, Brazil, the M.S. degree from the Federal University of Rio de Janeiro (UFRJ),Rio de Janeiro, Brazil, and the Ph.D. degree from the Federal University of Paraíba (UFPB), João Pessoa, Brazil, in 1979, 1982, and 1997, respectively, all in electrical engineering.

He is a Full Professor in the Department of Electrical Engineering, UFBA. His research interests include electronic instrumentation, particularly in measurements systems, thermo-sensors, and signal processing for measuring purposes.